

https://dspace.org/

PIXE SEM and RAMAN analysis of pictorial materials from the VIII century crypt of San Salvatore Brescia Italy

Alessandro Zucchiatti; Stefano Roascio; Inmaculada Donate Carretero; Paolo Antonino Maria Triolo

SPRINGER HEIDELBERG
https://hdl.handle.net/10539/43456
WOS

Downloaded from a DSpace repository. https://dspace.org/

Eur. Phys. J. Plus (2024) 139:1015
https://doi.org/10.1140/epjp/s13360-024-05800-0

THE EUROPEAN PHYSICAL JOURNAL PLUS

Regular Article

PIXE, SEM and RAMAN analysis of pictorial materials from the VIII century crypt of San Salvatore, Brescia (Italy)

Alessandro Zucchiatti[1,2,3,a], **Stefano Roascio**[4,b], **Inmaculada Donate Carretero**[5,c], **Paolo Antonino Maria Triolo**[6,d]

[1] School of Physics, University of the Witwatersrand, Johannesburg, South Africa
[2] Dep.to de Prehistoria y Arqueologìa, Universidad Autònoma de Madrid, Madrid, Spain
[3] Dip. to di Scienze della Terra dell'Ambiente e della Vita – DISTAV, Università Di Genova, Genoa, Italy
[4] Parco Archeologico dell'Appia antica, piazza delle Finanze 1, 00185 Rome, Italy
[5] Servicio de Conservación, Restauración y Estudios Científicos del Patrimonio Arqueológico (SECYR), Universidad Autónoma de Madrid (UAM), Madrid, Spain
[6] Dip. to di Italianistica, Romanistica, Antichistica, Arti e Spettacolo – DIRAAS, Università Di Genova, Genoa, Italy

Received: 28 July 2024 / Accepted: 4 November 2024
© The Author(s) 2024

Abstract The complex of Santa Giulia of Brescia (Italy) is a great and extensively studied architectural and archaeological site, of which the church of San Salvatore is an emblematic monument. This study, conducted in the crypt of the church, implements what was published from non-destructive particle induced x-ray emission (PIXE) examination of the painting materials with structural and compositional analyses by Scanning Electron Microscopy and Raman spectroscopy. These analyses produced new and decisive data for a correct identification of the pictorial palette. We also added a photographic documentation in a few bands of the electromagnetic spectrum. The review of all data and their complementarity has allowed a more sound insight into the pictorial techniques used for the crypt's decoration. This work integrates the archaeological studies conducted on the crypt and, together with them and in comparison with data from coeval monuments, confirms in the church of San Salvatore the use of products and techniques typical of the Longobard Period.

1 Introduction

The women's monastery of Santa Giulia was founded in 753 AD by the future Longobard king Desiderius on an area near the Capitolium of the Roman town of Brixia, that hosted important houses *(domus)* of the Roman era. It has evolved since, with the addition of several buildings and nowadays is part of a monumental complex, which is the site of the major museum of the city of Brescia. The complex includes the Longobard Basilica of San Salvatore, first erected in seventh century, its crypt, the Romanic oratory of Santa Maria in Solario, the nuns' choir, the fifteenth century church of Santa Giulia, the cloisters.

The crypt, object of this study, belongs to the so-called San Salvatore second church, inaugurated in 761 AD. The church transformation consisted in a huge extension that moved the three apses 6 m to the east and in the removal of the transept to leave place to two new lateral naves. King Desiderius's family conceived the renewal as a dynastic mausoleum, connected to the royal cloister, whose importance was marked by having received a pontifical concession to host the remains of the Christian martyr saints Giulia, Pistis, Elpis and Agape. The crypt at present is composed of two different spaces (Fig. 1): the first, belonging to Early Middle Ages, corresponds to the middle apse and the side arcs, while the space in front, featuring three rows of columns, dates from the middle XII, XIII century.

Several scholars have studied the monumental complex in detail, producing relevant reports: e.g., the UNESCO World Heritage List Nomination Format [1] and the comprehensive review of the architectural structures and the restorations history [2]. Important studies have been conducted by P. Brogiolo [3] who co-authored as well the first account of our study of the crypt, where we presented a detailed description of the crypt architectural structure [4] and its decorations, as well as a discussion on the employed materials and a first report of their instrumental analysis.

The sole use of PIXE [4], gave us a general overview of the materials that were employed but was not decisive in defining the pigments nature. First because of its limited spatial resolution (although relatively good for a proton beam in air) and because we

[a] e-mail: sandrozucchiatti@gmail.com (corresponding author)
[b] e-mail: stefano.roascio@cultura.gov.it
[c] e-mail: inmaculada.donate@uam.es
[d] e-mail: paoloantoninomaria.triolo@unige.it

Published online: 22 November 2024

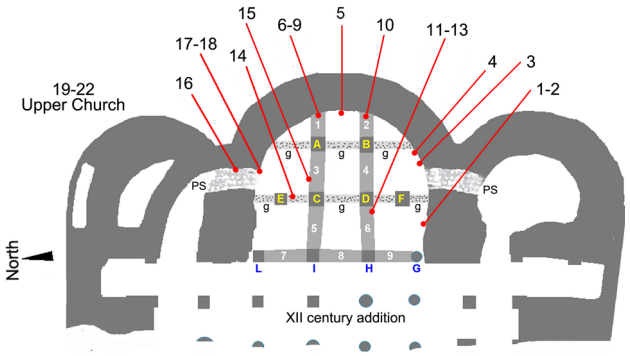


Fig. 1 The Crypt plan with the indication of the sampling areas. Capital letters indicate pillars and columns. Numbers indicate arches. Girders are identified by the letter "g" and the ancient access passages by "PS"

could not use its imaging power. Secondly because of the completely altered state of the samples, specifically those buried for centuries in the crypt.

Recently we had the opportunity to expand our analyses, by permission of "Ministero della Cultura– Soprintendenza Archeologia, Belle Arti e Paesaggio per le Province di Bergamo e Brescia" (0014967 dated 20/07/2022). The scope of this paper is to deepen the analysis at microscopic level and summarize what we have learned on the pictorial, decorative and preparation materials employed in the crypt.

2 Sampling

At an early stage (2004–2005) of the crypt last restoration campaign, we collected samples in the millimetre range, having care at extracting, whenever possible, both the pictorial surface and the preparation underneath, while keeping to minimum the quantity removed. Samples were duly returned to the Soprintendenza Archeologica after extended particle-induced x-ray emission (PIXE) analysis. However, the few very small fragments that detached from the brittle original samples (and we retained) were sufficient to apply, years after, microscopic techniques like scanning electron microscopy (SEM–EDS) and micro Raman spectroscopy seeking for new complementary results.

A total of 18 samples came from the crypt; their location is indicatively shown in the plan of Fig. 1 and the photos of Fig. 2. The colour palette is limited to a few shades of red (including sinopite) and yellow as well as black and grey. We sampled also a stucco decoration in the north central arch. Four more samples, including a green one, have been taken in the upper church northern wall but they were not considered in the previous report [4]. Table 1 shows the complete list of samples and relative measurements. Figure 2 shows examples of the aspect of the walls surfaces, in connection with the sampled areas.

The examination of samples by a stereo microscope revealed that their structure, by construction and deterioration with time, is complex with phases intermixed and altered, which will be reflected in the difficulty of interpretation of some of the obtained results.

3 Analytical methods

3.1 Particle induced X-ray emission (PIXE)

We performed PIXE at the AGLAE accelerator of the Centre de Recherche et Restauration des Musées de France (C2RMF). A 3 MeV proton micro-beam extracted in air through a ultra-thin (100 nm) silicon–nitride window was delivered to the sample, where it covered a disc of roughly 50 μm of diameter [5]. The interaction of the protons with the atomic electrons in the sample generates X-rays, which are characteristic of the atomic species. They were collected by a two-detector system: their energy identifies the element and their yield leads to its concentration. The X-ray energy spectra were deconvoluted by the software package GUPIX [6] that assumes homogeneous samples, eventually consisting of homogeneous layers, and calculates the elemental oxide concentrations, from Na onward, through an iteration process. Results are controlled in a way identical to that adopted in previous analyses [7–9], that consists in repeatedly measuring a set of glass reference materials produced by Brill [10] and the British Glass Industry Research Association [7–9]. Supposing that the origin of the samples is mineral we imposed that all the elements are found in the oxide form, except calcium which was supposed to come in the form of $CaCO_3$, as it should be for frescoes. For the *stucco*, the analysis has assumed that all elements are in oxide form since $CaSO_4 = CaO + SO_3$.

With an external micro-beam raw samples can be analysed without preparation. Considering the typical structure of a fresco decoration and the size of our collected samples, we could easily perform PIXE analyses either from the painted surface or the side of the wall preparation (*intonachino*). In both cases, we are sure that the proton range in the material (a few tens of microns) is



Fig. 2 The location of the samplings in the crypt and the upper church. Photos taken by concession of Soprintendenza Archeologia, Belle Arti e Paesaggio per le Province di Bergamo e Brescia. They cannot be reproduced or duplicated by any means

below the thickness of the painted layer and the preparation which the code GUPIX assumes homogeneous. In surfaces of complex structure like ours, it is possible to aim at single points or to scan the sample over an area to obtain a signal averaged over the composition in both surface and depth (proton range). Furthermore, with layered samples, it is possible to explore the layers and eventually scan them over a line, provided that the beam positioning can be accurate enough to avoid layers admixture and embedded mineral grains (e.g. silica) within the 50 μm of the beam spot. To overcome the spatial resolution limits of the PIXE, a few of the 22 samples have been incorporated into resin and the cross section has been polished to allow new complementary scanning electron microscopy (SEM), which is reported below. About half the reported PIXE results were obtained from spot analyses and the rest from either surface or linear scans. As seen in Table 1, PIXE is the technique that provided the widest characterization of the samples, both because all the samples were available for analysis and their easy handling, in air, allowed to characterize more parts of their structure. We performed 114 measurements on the 22 collected samples intermixed with 50 measurements on glass standards for repeated calibration.

Table 1 The list of samples, with colour and the analysis techniques employed for each sample

Sample	Colour	PIXE	SEM	Raman
Right wall of the crypt central apse				
1	Black and yellow (in the volute)	x		x
2	Black and yellow (in the volute)	x	x	x
3	Yellow (after a wall aperture)	x	x	x
4	Red	x		x
5	Dark Yellow (of the front specchiatura)	x		
6	Preparatory yellow	x		x
7	Preparatory yellow (high spot)	x	x	x
8	Preparatory yellow (high spot)	x		
9	Red (poppies)	x	x	x
10	Yellow (arch bottom)	x		x
South West Arch bottom (oldest building phase)				
11	Yellow	x		
12	Red	x		x
13	Wine red	x		x
Western Girder				
14	Yellow (bottom)	x		x
North Central Arch				
15	Stucco	x		x
North Passage East side				
16	Sinopite (whitewashing)	x	x	x
17	Mortar (original plastering)	x		
18	Mortar (specchiatura)	x		
Upper Church North perimeter				
19	Red	x		x
20	Yellow	x		x
21	Grey	x		x
22	Green	x	x	x

3.2 Scanning electron microscopy coupled to energy-dispersive spectrometry (SEM–EDS)

We analysed embedded samples using the scanning electron microscope (SEM VEGA3 TESCAN) of the Department of Earth, Environmental and Life Sciences (DISTAV) of the University of Genoa. The instrument is equipped with a thermo-ionic filament that allows a resolution of 3 nm at 30 kV and 8 nm at 3 kV, with probe current from 1 pA to 2μA, capable of magnifications from 2X to 10^6X. For imaging, it is equipped with ET-SE and BSE detectors. Element's characteristic X-rays are collected by an EDAX Apollo XSDD detector with DPP3 electronics, associated with the TEAM (Texture and Elemental Analytical Microscopy) analysis software. The SEM operated at an acceleration voltage of 20.0 kV, a working distance of 15.00 mm, with measurement times varying from 50 to 100 s.

SEM–EDS gave, with spatial resolution much better than PIXE, complementary information on the colours nature and sample structure. We performed a total of 34 measurements on 6 embedded samples.

3.3 Raman spectroscopy

We used a B&WTEK spectrometer, model i-RamanPro 785, of the Servicio de Conservación, Restauración y Estudios Científicos del Patrimonio Arqueológico (SECYR), Universidad Autónoma de Madrid. The instrument is provided with a sampling fibre optic probe BAC-102-785E, which can be used as a manual probe for in situ measurements or, as in our case, connected to an optical microscope with enlargements from 20X to 100X. Raman spectra, produced by the 785 nm wavelength incoming light, are collected by a high quantum efficiency CCD array detector, with deep cooling (-25 °C) and high dynamic range, that measures down to 65 cm^{-1} and up to 3350 cm^{-1} with a resolution of 4.5 cm^{-1}.

Table 2 reports experimental conditions for the San Salvatore spectra shown in Figs. 9, 10, 11, 12 and 13. With the 50X enlargement adopted we have measured a maximum power on sample of 265 mW. The system allows to select the percentage of maximum power in steps of 1%.

Data collection is supported by the BWSpec software. ASCII data can be transferred to any plotting and data analysis package.

Table 2 The list of San Salvatore samples included in Figs. 9, 10, 11, 12 and 13 with the corresponding experimental conditions

Figure	Sample/measure	Magnification	Step Time [s]	Repetitions	Power [mW]
9	SP-9–1 Red	50×	10	3	13.25
	SP-6–1 Yellow	50×	10	3	5.3
	SP-22–1 Green	50×	30	4	7.95
	SP-16 Sinopite	50×	30	4	10.6
10	SP-21-BK1	50×	30	4	5.3
	SP-21-BK2	50×	30	4	7.95
	SP-14-CZ	50×	30	5	7.95
	SP-20-CZ	50×	30	5	13.25
	SP-14A-BK	50×	30	4	7.95
11	SP-12–1	50×	30	1	21.2
	SP-13–1	50×	30	1	21.2
12	SP-15–1	50×	30	3	7.95
	SP-15–3	50×	30	3	15.9
	Sp-15–2	50×	30	5	7.95
13	SP-1–1	50×	30	4	10.6
	SP-2–1	50×	30	3	21.2

Raman spectroscopy has provided clearly identifiable peaks to determine the nature of the examined materials, in some cases but not in all. A total of 70 spectra have been analysed in 17 samples. The spectrometer calibration has been verified with gypsum ($CaSO_4 \cdot 2H_2O$) and cinnabar (HgS) SECYR reference materials.

3.4 Photography

First we produced photographic documentation in diffused visible light, with a standard Nikon D800 camera, using a Macbeth X-Rite Classic Color chart as reference. Light was supplied by a Nikon SB610 flash, the lens was a Nikkor 50 mm 1:1.8G, and the shooting parameters were ISO100, f7.1, 1/125".

We performed in addition infrared reflectography in the range 780 nm-980 nm (NIR). The technique may give information regarding the presence of preparatory traces and repentances, otherwise not perceptible. It may also produce indications regarding the executive-pictorial practice, leading to the identification of technical characteristics and specific peculiarities of the pictorial ductus. Sometimes, the comparison between NIR and ultraviolet fluorescence allows us to identify interventions of a mimetic nature.

For NIR, we used a modified Nikon D800 IRUV digital camera. The hot mirror filter of the standard camera has been removed and the camera is equipped with Schott WG280 quartz filter [11], with a 35.9 mm × 24 mm SLR 36.3 MP CMOS (7360 × 4912 Pixels). We mounted a Nikkor 50 mm 1:1.8G lens with and IR filter PECA 910 (87C) IR.

We also exploited visible-light-induced infrared luminescence (VIL) [12–16]. This particular type of fluorescence may indicate the presence of Egyptian blue, Roman blue, Maya blue, Han blue and purple, cadmium-based reds and oranges. Associated with a specific filter it also provides information on conservative interventions. The investigation was carried out again with a modified Nikon D800 IRUV camera, equipped with a Nikkor 50 mm 1:1.8 g lens provided with a PECA 87c filter. Illumination was provided by a Madatec 630 nm red LED projector. Shooting parameters were ISO100, f7.1, 1/125″. We used as reference a color chart Rite Classic and a Egyptian blue Kremer 10,060 tablet.

4 Results and discussion

4.1 PIXE analysis

Confirming the microscopic observations, the PIXE analyses reveal that preparations consist of magnesic lime loaded with inert silica (Fig. 3). The weight concentration ratio is $MgO/CaCO_3 = 0.17 \pm 0.09$ (standard deviation) while $SiO_2/CaCO_3 = 0.13 \pm 0.08$. The degradation of the pictorial surface, already evident on site (Fig. 2) is confirmed by the PIXE results. From the data, we have calculated the CaO/SO_3 both when measuring from the preparation side (Fig. 4 left) and from the painted surface (Fig. 4 right). We calculate CaO as $CaO = 0.56 \times CaCO_3$ without taking care of the marginal effects that a different matrix will have on GUPIX iteration method. In the coloured surface, CaO/SO_3 is between 0.66 and 2.95 with an average of 1.1 ± 0.4.

The stoichiometric value from a pure calcium-sulphate would be 0.7; the data show the important presence of gypsum in the samples surface either as a degradation product or a basic ingredient [17, 18]. In the preparations, the calcium carbonate remains

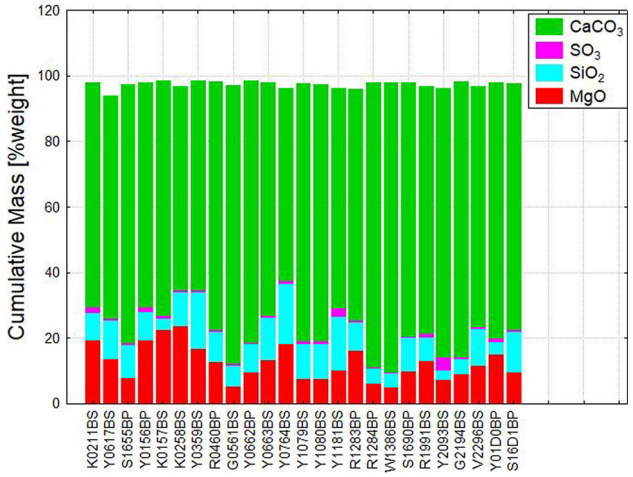


Fig. 3 The cumulative mass of the four major components of the "intonachino". Labels of the X-axis are the measure code

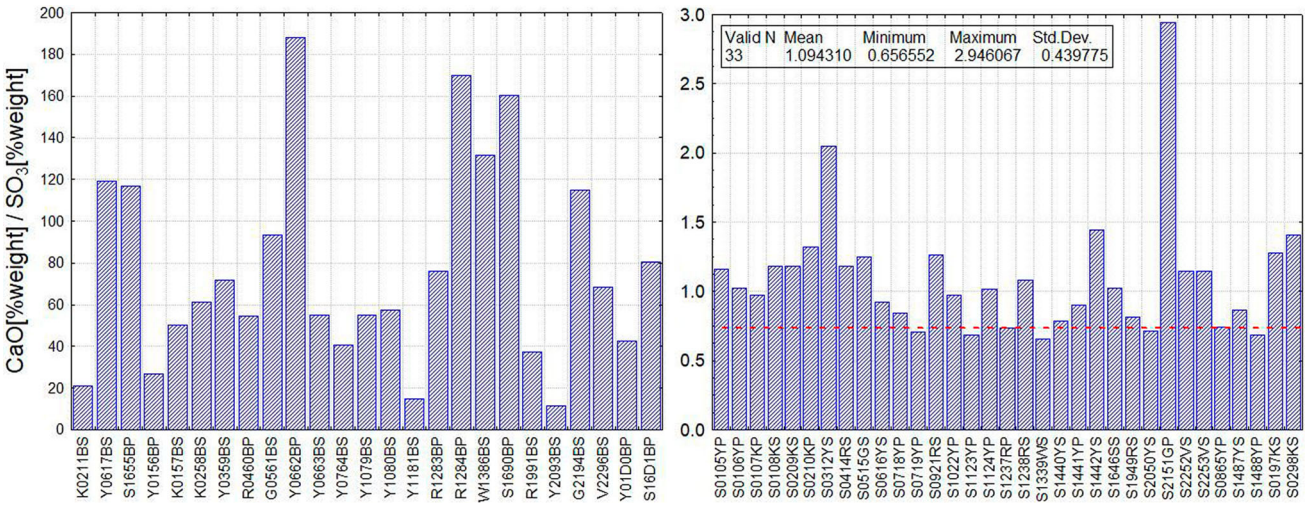


Fig. 4 The CaO/SO_3 ratio measured on the sample from the preparation side (left) and the painted surface (right). Dotted line indicates the stoichiometric value of $CaSO_4$. Labels of the X-axis are the measure code

predominant. The degradation carbonate-sulphate is a common occurrence and has been already observed, e.g., in other frescoes from the Longobard times. [19].

Concerning the painted surfaces, the amount of elements characteristic of specific pigments is quite variable. However, some indications have emerged from the PIXE analysis.

The largest group of analyses has been performed on yellow and red pigments. Figure 5 gives the distribution of element oxides concentration in four groups of samples, in the box and whisker format. The symbol indicates the average value, the box covers from 25 to 75% of the samples and the whiskers mark the minimum and maximum without outliers.

Reds and all the yellow samples, with the exception of sample 14 (coded as YellowPb), have Fe as the most abundant element. In addition, Na, Al, and K are present, suggesting that the red and yellow pigments are ochres. The wine-red sample, was analysed only once but the relatively high Fe, Na and Al suggest again an ochre. Mercury does never appear in the red pigments, which excludes cinnabar as a possible ingredient.

Sample 14 comes from the western girder and belongs to a pictorial phase later than the other yellows but still previous to the Renaissance reconstruction [4]. The sample (a parallelepiped $2 \times 3 \times 3$ mm^3) showed a rather peculiar layered structure [4]. The outer layer, quite thick and perhaps double, was followed by a preparation that seemed to stand on a previous yellow pictorial layer, thinner and lighter than the outer one. The sampling seemed to have produced a fracture right along this inner painted layer. The PIXE measurements from the surface of the two painted sides indicate the presence of Pb (Fig. 5) on one surface that should have been painted with a lead yellow, perhaps not as a fresco. Unfortunately, only a little fragment of the sample remained available for further analysis but it was not possible to establish from which of the original layers it had fallen.

In black and grey samples (Fig. 6), the most abundant oxides are Na_2O, Al_2O_3, Fe_2O_3 but their maximum value remains below 1%. Black samples contain also K_2O and PbO. K_2O has values between 0.02 and 0.24% and median 0.11%. PbO has values from 0.07 to 0.27% with average 0.14% while MnO and TiO_2 are only at trace level. The dark black colour appears to be of organic origin.

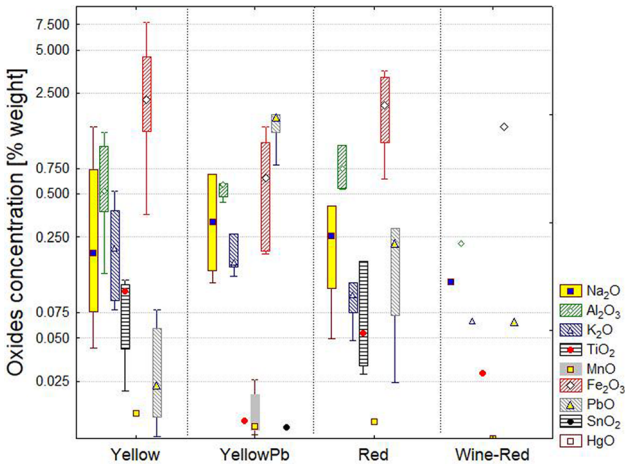


Fig. 5 The distribution of oxides concentrations in yellow and red samples

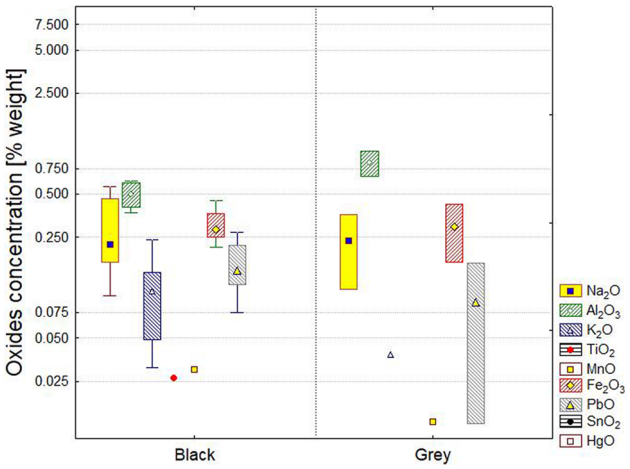


Fig. 6 The distribution of oxides concentration in black and grey samples

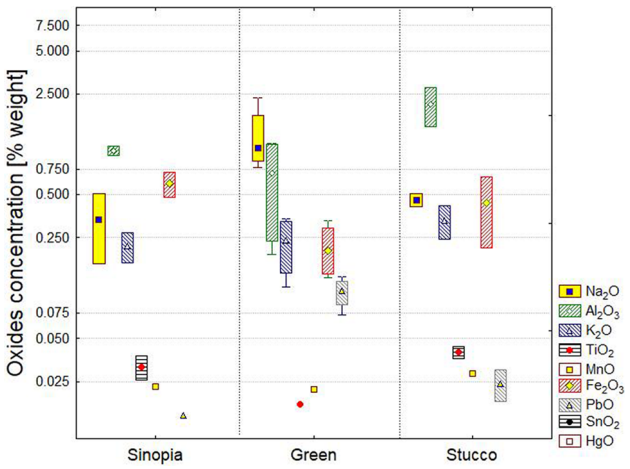


Fig. 7 The distribution of oxides concentration in sinopite, green and stucco samples

In the grey sample, K_2O and PbO are even lower that in the black ones. As it will be discussed later, thanks to the new SEM–EDS results, PbO in the black samples is to be ascribed to surface contamination.

Three more materials were analysed. A sinopite (Sinopia), a green sample from the upper church and a "stucco" from the north central arch (Arch #3 in Fig. 1, sample 15 in Table 1). When the sinopite sample was collected, the pigmented layer appeared rather thin and degraded. Indeed, we were not able to precisely align the beam with a sinopite spot and the measurements we have taken do not clearly identify the nature of the earth. Oxide concentrations seem comparable to those found in black, grey and red samples but Fe_2O_3 is much lower than in red samples confirming the impression that the pigmented layer was much degraded. No PbO was present.

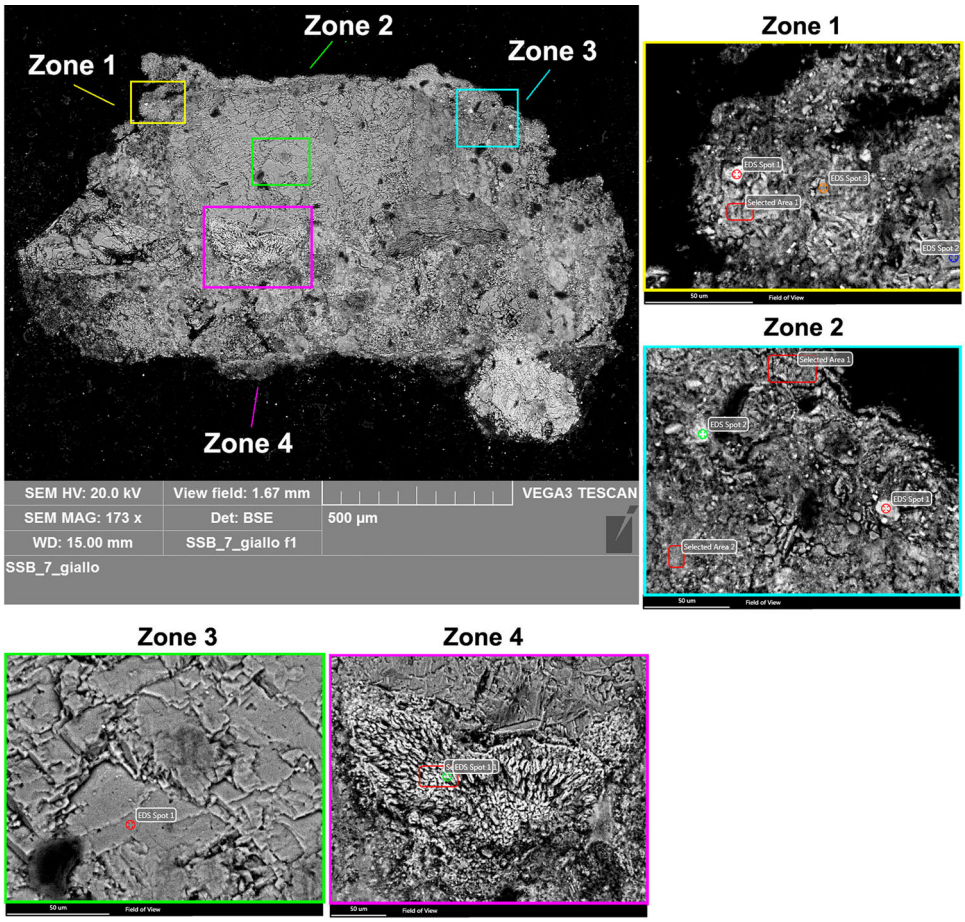


Fig. 8 Cross section of Sample 7, yellow. Enlargements, marked by colour frames, are shown with indication of points or areas measured by SEM–EDS

The green sample, collected in the upper church, confirms the compatibility of technique and materials with the grey, yellow and red samples collected in the crypt and belonging to an earlier pictorial phase. PIXE (Fig. 7) indicates that the pigment should correspond to a green earth having (in the order) Na_2O, Al_2O_3, K_2O and Fe_2O_3. PbO is a minor component ranging from 0.07 to 0.14% and median 0.11%. Previous extended analyses of green earths (e.g. [20, 21] have excluded the presence of Pb in such pigments. As for the black and grey samples, SEM–EDS has demonstrated that PbO is to be considered as a surface contaminant.

The "stucco" decoration sample comes from a pictorial phase previous to the Renaissance reconstruction. Its composition, analysed by a beam-scan over a 1×1 mm^2 area, gives an average value $CaO/SO_3 = 0.66$ very close to the stoichiometric value (0.7) of calcium sulphate.

4.2 Scanning electron microscopy

A few samples, embedded in resin and analysed by PIXE, were further characterized by SEM–EDS: samples 22 (green), 2 (black), 3 and 7 (yellow), 9 (red) and 16 (sinopite).

Figure 8 shows the enlargements and the measurements performed on sample 7, while Table 3 gives the composition measured in the five samples and in different points (p) or scanned areas (A). Nowhere in the SEM analyses of polished sections Pb has been above detection limits, which suggests that in the PIXE analyses it came from surface contamination produced during centuries of contact with fill land.

Magnesic calcium carbonate (dolomite) as well as calcium carbonate and gypsum are regularly found in all samples. Fe is found in high quantities in yellow and red samples as well as in sinopite. The black sample contains, besides calcium carbonate and sulphate, inclusions of ilmenite and biotite. However, the parts that under visible light appear black are simply dominated by the carbon peak at 0.28 keV.

In the green sample, one of the measured points (S22-G-Z2-p1) can be associated to a genuine green earth pigment. It has a high content in magnesium, aluminium, potassium and iron, but relatively low calcium. According to both the criteria adopted by Hradil [22] – K/(Si/Al) ~ 2 – or by Ospitali [23] – Si > Al > Mg – the green earth should be glauconite. Our result was K/(Si/Al) = 2.27.

No Pb has been detected by SEM–EDS on the green sample. Again the small amount of Pb (max. 0.14%) found by PIXE is to be ascribed to surface contamination. The green sample comes from one of the few patches of the original frescoes recovered on

Table 3 The composition measured by SEM–EDS in points or scanned areas of six samples from the crypt

Sample, Zone, Point	Na_2O	MgO	Al_2O_3	SiO_2	P_2O_5	SO_4	Cl	K_2O	CaO	TiO_2	Cr_2O_3	MnO	FeO	CuO	ZnO	SrO	Nb_2O_5	Total	Interpretation
S22-G-Z1-A1	0.4	7.96	0.31	1.06	0.3	5.94	0.3	0.12	28.8				0.28					45.43	$CaCO_3$ + dolomite + $CaSO_4$ + Fe oxide
S22-G-Z1-p1	0.06	14.31	0.22	0.5	0.26	2	0.19	0.09	26.4									44.06	$CaMg(CO_3)_2$ (dolomite) + CaSO4
S22-G-Z2-p1	0.35	8.88	17.61	47.1	0.53	0.22	0.14	6.47	1.29	0.26			4.45					87.28	Mostly Green earth
S2-B-Z1-p1	0.72	1.99	35.36	45.1		0.26	0.12	8.69		0.27			2.57					95.04	Biotite (mica)
S2-B-Z2-p1	0.1	8.42	24.82	24.4				0.16	0.13			0.19	32					90.22	Fe oxides?
S2-B-Z3-p1		1.81	0.11	0.95	0.29	0.66	0.13	0.06	50.7									54.66	Mostly $CaCO_3$ + dolomite
S2-B-Z4-p1	0.1	4.78	6.96	14.5		0.35	0.18	0.38	1.7	4.75		0.21	50.3					84.24	Fe oxides + $FeTiO_3$ (ilmenite)
S2-B-Z4- p2																			spectrum dominated by C peak
S2-B-Z5-A1		1.49	0.33	2.04	0.25	27.4	0.24	0.17	33.1	0.12			0.36					65.45	$CaCO_3$ + $CaSO_4$
S2-B-Z5-p1	0.23	1.13	0.11	0.75	0.46	51.5	0.41	0.31	34.2									89	Mostly $CaSO_4$
S3-Y-Z1-p1	0.18	11.18	12.38	31.7	0.36	8.64	0.58	4.41	5.04	0.49			12.3	0.54	0.32			88.12	Yellow ochre + $CaSO_4$
S3-Y-Z1-p2	0.37	2.84	0.25	5.43	0.21	55.1	0.13	0.2	35.2				0.23					100	Mostly $CaSO_4$ + Silica
S3-Y-Z1-p3	0.19	0.44		0.28		2.59			50.5				0.23			0.59		54.8	Mostly $CaCO_3$
S3-Y-Z1-p4	0.33	2.7	0.49	1.52	0.43	8.03	0.2	0.16	37.8	1.78			9					62.46	dolomite + $CaSO_4$ + Fe oxides
S7-Y-Z1-A1	0.48	4.04	1.19	4.95	0.41	51.4	0.23	0.31	30.4				1.68					95.04	Mostly $CaSO_4$ + Yellow ochre
S7-Y-Z1-p1	0.31	6.97	4.06	7.89	1.31	0.56	0.28	0.21	0.68	0.46	0.06		51.3					74.08	Fe oxides + Yellow ochre
S7-Y-Z1-p2		21.36							31.2									52.58	$CaMg(CO_3)_2$ (dolomite)
S7-Y-Z1-p3	0.13	5.99	0.78	6.35	0.18	55.6	0.27	0.1	36.9				0.8					107.1	Mostly $CaSO_4$ + dolomite + silica
S7-Y-Z2-A2	0.41	7.08	0.45	4.1	0.45	1.04	0.15	0.12	34.8				0.25					48.87	CaCO3 + dolomite + silica
S7-Y-Z2-A1	0.14	6.12	0.6	6.31	0.26	43.7	0.3	0.13	28.2				0.35					86.03	Mostly CaSO4 + dolomite + silica
S7-Y-Z2-p1	0.35	4.51	1.9	6.23	1.1	0.48	0.2	0.33	1.41	0.35		0.19	41.6					58.69	Fe oxides + Yellow ochre
S7-Y-Z2-p2	0.31	7.01	3.43	9.82	1.44	0.58	0.18	0.32	1.15	0.6	0.08	0.12	49.9					74.94	
S7-Y-Z3-p1		17.93							31									48.96	$CaMg(CO_3)_2$ (dolomite)
S7-Y-Z4-A1	0.56	1.72	0.29	0.5				0.25	48.1				0.57			0.51		52.52	Mostly CaO + dolomite
S7-Y-Z4-p1	0.21	0.72	0.06	0.14				0.09	46.9							0.36		48.46	
S9-R-Z1-p1		12.8	27.59	27.3				0.14	0.42	0.25		0.23	31.4					100.1	Red earth
S9-R-Z1-p2		2.18	1.74	2.23				0.11	1.69	83.7			2.02				0.32	93.95	Ti oxide
S9-R-Z2-A1		0.31	0.14	0.22	0.37	63.6			31.2				0.31					96.05	Mostly $CaSO_4$
S9-R-Z2-p1	0.43	7.42	1.59	4.99		2.03	0.19	0.17	3.18	0.38			58.3					78.7	Mostly Fe oxides
S9-R-Z2-p2	0.44	9.52	4.28	12.3	0.68	10.8	0.24	0.51	7.91	0.29		0.1	52					99.09	Fe oxides + dolomite + $CaSO_4$
S9-R-Z2-p3																			Spectrum dominated by Ca peaks
S9-R-Z3-p1	0.35	2.55		2.64	0.14	0.67	0.38	0.11	2.47			1.42	65.4					76.09	Fe oxides
S16-S-Z1-A1	0.34	2.07	0.88	3.88	0.61	1.66	0.18	0.25	30				4.47					44.31	$CaCO_3$ + dolomite + $CaSO_4$ + Fe oxides
S16-S-Z1-p1		0.21	0.13	0.61		0.62		0.11	1.79			0.46	75.5					79.45	Fe oxides

Coding example: S16-S-Z1-p1 –> Sample 16—Sinopite (Y, yellow; B, Black; G, Green; R, Red; S, Sinopite)—Zone 1—Point 1 (p, point; A, area)

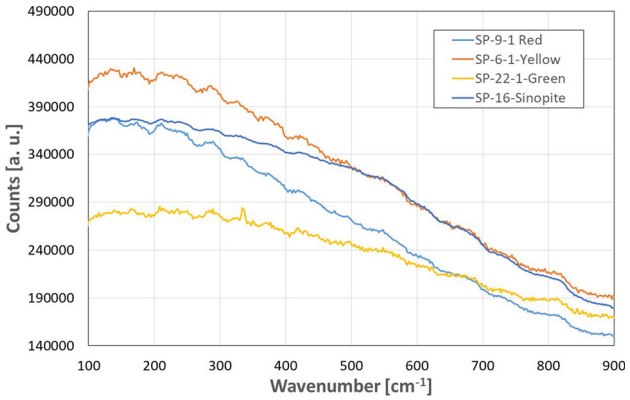


Fig. 9 The most frequent spectrum aspect observed for various colours

the north wall of the upper church, where the hammering, clearly visible in Fig. 2, demonstrates that, besides the loss of a large part of the frescoes, the surface was prepared to be plastered and maybe repainted.

4.3 Raman spectroscopy

Scanning electron microscopy has shown how complex is the structure of the collected samples, due to the pictorial technique and to the degradation that the painted surface has experienced, in centuries of abandonment in contact with the wet soil, which filled up the crypt. This has made difficult the execution of Raman spectroscopy on the samples. However, a few confirmations came from the analysis, namely:

a) In many spectra, the fluorescence builds up (Fig. 9) a large background over which a series of broad peaks appear, as a consequence of the complex nature of the samples as confirmed by the microscopic observation (both optical and electron).
b) The degradation process that transforms calcium carbonate into calcium sulphate is demonstrated in many samples by the presence, at different intensities, of both the band 1008 cm^{-1} of gypsum and the band 1084 cm^{-1} of calcium carbonate (Fig. 10).
c) The red colour shows clearly the signal of haematite (comparison with the RRUFF haematite standard R040024) in samples 12 and 13 (Fig. 11). They belong to the crypt's western arch that featured the best preserved red colours (Fig. 2). Also sample 9 shows the characteristic peaks of haematite but at lower intensity with respect to the background.
d) The "stucco" collected in the north central arch is the most homogeneous material of the many collected. It consists of gypsum (comparison with SECYR gypsum reference material). No organic compounds, like egg white are observed (Fig. 12).
e) In our black samples, we observe (Fig. 13) two peaks compatible with the D and G bands of several carbon compounds observed in literature [24–26], taking into account the known variability of data. It has been observed [26] that "The D band showed a larger range of values (from 1345 to 1394 cm^{-1}) than the G band (from 1578 to 1603 cm-1)". Due to the absence of the 2662 cm^{-1} peak observable in the RRUFF R050503 standard, our samples are not compatible with graphite. Their microscopic SEM observation tells that they are also not compatible with other pigments available at the time of the crypt decoration. Tomasini et al. [27] report "amorphous crystals tending to be angular" (for ivory black);"crystals of 1–2 μm in size and small globular particles with a rough surface" (for vine black); "cell wall structures, channels and holes" (for charcoal); "an amorphous structure and a few irregular-shaped crystals" (for bistre) and "particles of 50–100 nm with pseudo-cubic shape" (for black earth). None of these features is observed in our black samples. They show (Fig. 14) small amorphous structures with smooth surfaces mostly ellipsoidal, sometimes elongated, that recall the lamp black SEM–EDS analysis of [27] that shows, as ours, the dominance of carbon (97.55%) and a texture consisting of spherical structures with smooth surface. Lamp black is the strongest candidate for the black pigment used in San Salvatore.

5 Photographic documentation

Standard colorimetric correction and image calibration were performed via Adobe Lightroom software [12, 28]; visible and infrared images are imported into Adobe Photoshop to produce false colour images [12]. This post-processing technique allows initial characterization of metameric pigments and, in case of infrared imaging, implies the mixing of the RGB channels of two coherent images of the subject, in visible and infrared band. Infrared image in greyscale is selected for insertion in the red channel of a new RGB image; the data from the red and green channels of the visible light image are inserted into the green and blue channels of the new image, thus obtaining the data in false colours. This in addition to the conventional false colour produced by the IR band between 780 and 980 nm (IRFC780-980 nm).

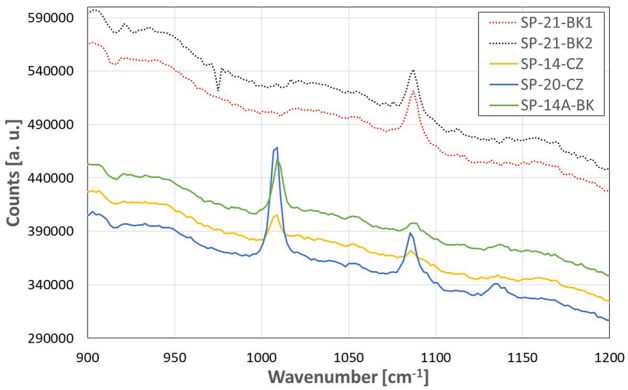


Fig. 10 The sulphate and carbonate peaks observed in samples examined from the back (SP-21-BK1, SP-21-BK2, SP-14A-BK) preparation and in surface parts (SP-14-CZ, SP-20-CZ) where the pigment was absent

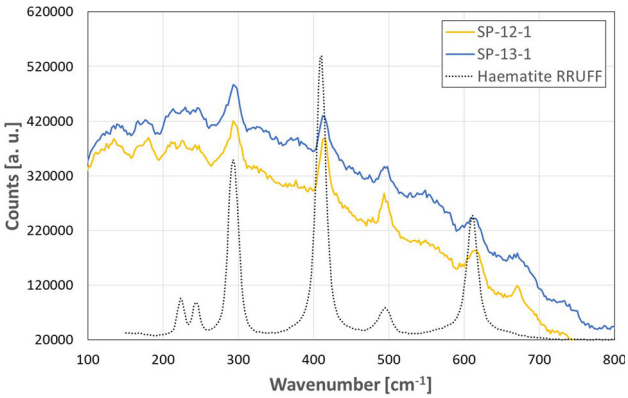


Fig. 11 The spectra of red samples SP-12 and SP-13, show the clear presence of haematite (standard RRUFF

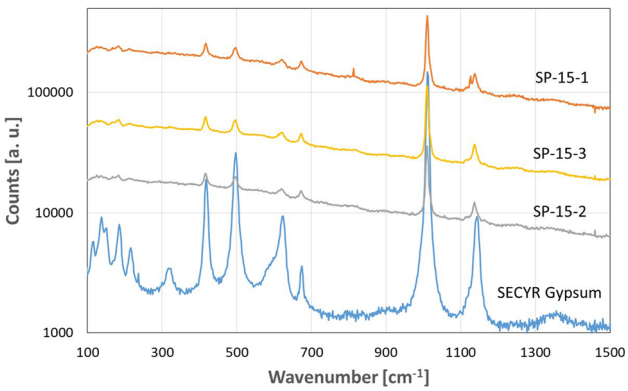


Fig. 12 The stucco sample SP-15 is homogeneous and consists of gypsum

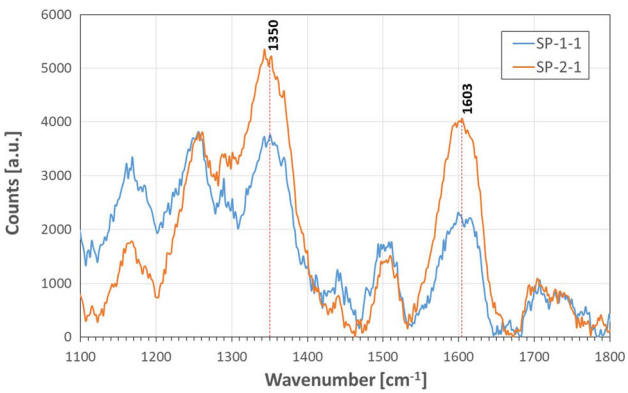


Fig. 13 The background filtered Raman spectra of black samples SP-1 and SP-2, show the carbon D and G band at 1350 cm^{-1} and 1603 cm^{-1}

The results of the multispectral acquisitions (Figs. 15 and 16) were aimed at determining the possible presence of Egyptian blue/Herculaneum blue ($CaCuSi_4O_{10}$). Two areas characterized by the presence of polychromy were chosen, corresponding to the

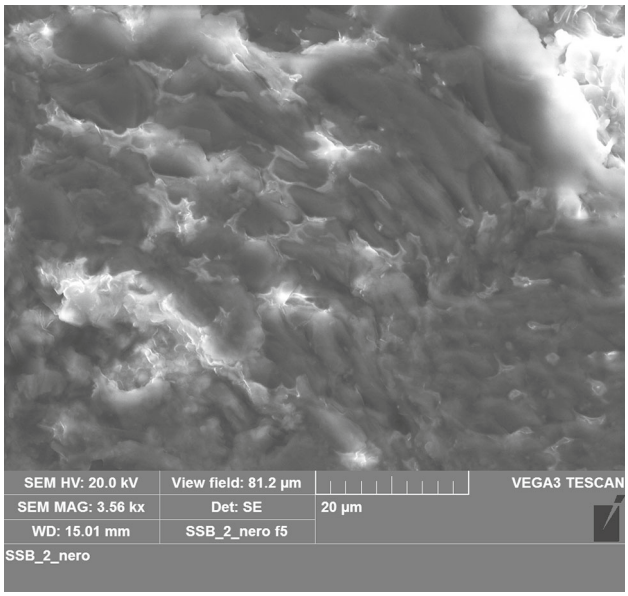


Fig. 14 At a microscopic scale the black sample SP-2 shows smooth, round or elongated structures, similar to what has been observed [27] for lamp black

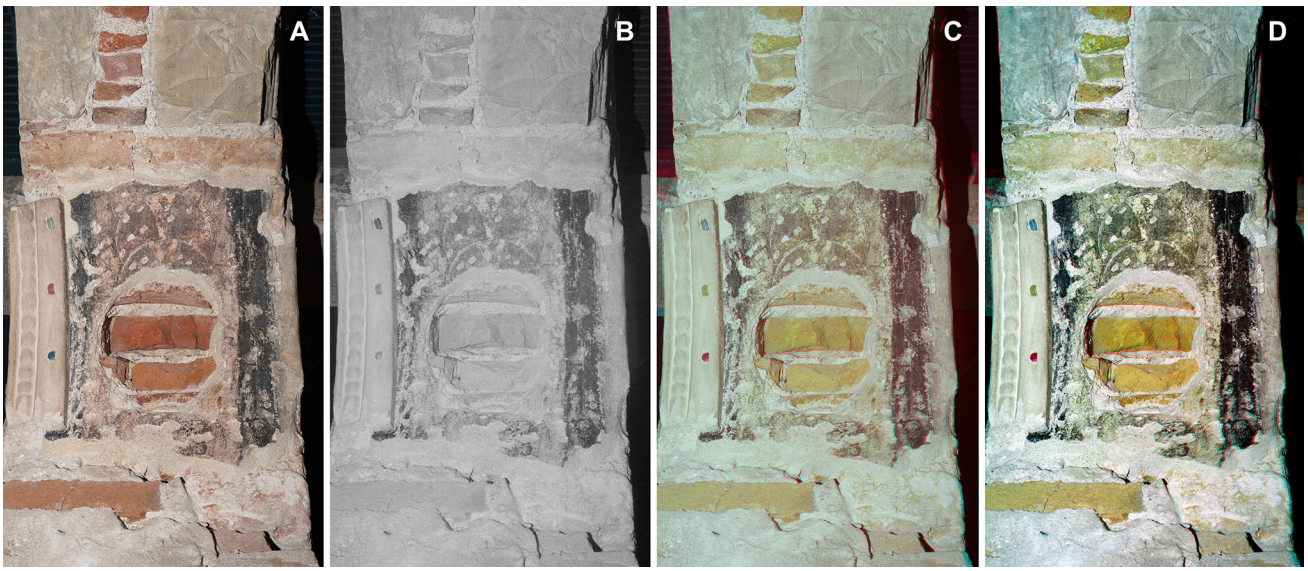


Fig. 15 Intrados of Arch 5. **A** Visible light (400-700 nm) D800 standard camera, flash light Nikon SB610. **B** Infrared reflectography (780-980 nm) D800 IRUV modified camera, PECA910 (87c) filter, flash light Nikon SB610. **C** IR False colours.**D** IR False colours (tonal compression postprocessing)

intrados of arch 5 and the lateral surface of arch 6 south (Fig. 1). The VIL luminescence was performed by inserting a tablet of Egyptian Blue Kremer 10,060, used as the maximum response index for carrying out the correct calibration during the acquisition and colorimetric correction phase.

No traces, backgrounds or residues of copper and calcium tetrasilicate were detected, which in VIL shows a characteristic and pronounced response, in a context of absence of signal from the pigments or surrounding materials.

Referring both to PIXE and SEM–EDS, copper – the element characterizing Egyptian blue but also other pigments such as azurite – is observed at a maximum of 360 ppm and average 97 ppm in PIXE (all colours included) and only in a single spot at 0.54% in SEM–EDS (Table 2). However, azurite is not applied in the carbonation phase (when wet), but only through an organic binder with dry technique.

In addition to the VIL luminescence, infrared and visible light shots were carried out for false colour processing and for the subsequent tonal contrast [28] by compressing the levels in Photoshop, which gave responses compatible with reds and yellows based on ochres and carbon-based blacks. The false colour did not detect any pink/red response that could be correlated to the set of blue pigments with a strong infrared response, which includes lapis lazuli, smalt, cobalt blue and Egyptian blue. However, we note the presence of three colored glass inserts in three different colors (green, red and blue) on the intrados. The blue one presents a false colour response of a pink/purple tone probably correlated to the presence of cobalt.

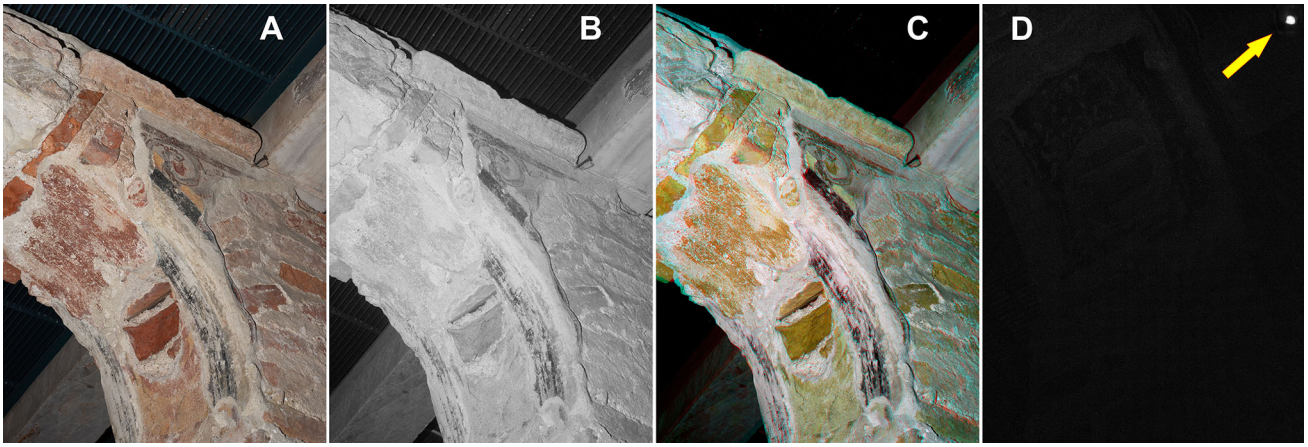


Fig. 16 Arch 6 south side. **A** Visible light (400-700 nm) D800 standard camera, flash light Nikon SB610. **B** Infrared reflectography (780-980 nm) D800 IRUV modified camera, PECA910 (87c) filter, flash light Nikon SB610. **C** IR False colours (tonal compression post processing). **D** VIL (visible induced infrared luminescence) D800 IRUV modified camera, PECA910 (87c) filter, Madatec 630 nm red led lamp. Egyptian blue (Kremer 10,060) reference on right top angle



Fig. 17 A few partial views of the crypt extracted from the photogrammetric model produced by the Agisoft MetaShape software

A series of images was also taken, aimed at creating a photogrammetric model. The 3D model was created via three-dimensional photo-modelling starting from a large photographic set in order to obtain both the three-dimensional model and any orthographic images for the correction of the two-dimensional photos (Fig. 17). The software used is Agisoft MetaShape. Further data processing is awaited in order to reconstruct the rest of the crypt.

6 Conclusions

The non-destructive PIXE technique, applied to raw as well as to some polished samples proceeding from the crypt of San Salvatore, had already given the oxide composition of the materials and offered a general comprehension of the materials employed in the crypt decoration. However the limitations of PIXE, as regards spatial resolution and mapping/imaging capability hindered a detailed definition of the nature of pigments.

With this study, we have overcome the limitations of PIXE by adding SEM–EDS, Raman analyses and photographic techniques to obtain decisive data for a correct identification of the pictorial palette. The entire set of data, including the samples from the upper church that were not considered in the previous work [4], has been reviewed.

The preparation of the walls for the realization of frescoes is similar in the crypt – in which we observed the first pictorial phases – and in the more recent upper church. The base of it is a magnesic calcium carbonate (dolomite) which in the painted surface is

degraded into sulphate in different, significant proportions. The effect of the long burial of the crypt makes the degradation more apparent in its earlier samples.

Pigments are among the most common and diffused at that time and similar in the crypt and the upper church. Red's are based on iron and in three occasions Raman could clearly identify haematite. Also yellow's are based on iron but the mineralogical structure could not be detected, although SEM–EDS has pointed out the presence of ochres. A distinct pictorial yellow phase was identified in a girder, featuring a lead-yellow and sulphate "stucco", probably an ancient restoration. Sinopite recalls a red ochre.

Thanks to SEM the green earth employed in the upper church has been identified as glauconite. Raman has clearly indicated that the black and grey areas have been obtained by using a carbon compound. Thanks to SEM we now know that is microscopically similar to lamp black observed in previous studies [27]. The "stucco" decoration is practically pure gypsum. No trace of organic components, like egg white, could be observed in its Raman spectrum.

NIR and VIL imaging, applied to large areas, have excluded that the black areas are degraded original blue areas. In addition, they point out that the blue glass, inserted with two more glass fragments in the stucco decoration of one of the arches, is most probably tinted with cobalt. A detail that wasn't known before.

In summary, this work supports the archaeological studies performed on the crypt and, together with them, confirms the use of products and techniques typical of the Longobard Period. Indeed, a similar palette of colouring materials and the use of stucco has been documented [29] in the coeval Longobard Temple of Cividale del Friuli, although the composition of the red and yellow ochres is different indicating a different source for the raw materials. In the case of Cividale, the use of false blue could be demonstrated by PIXE micro-mapping, which was not used for San Salvatore.

The pictorial palette and the execution techniques, although completely compatible with the period, did not however provide discriminating elements for particular technical processes, typical of a definable pictorial tradition. Instead, this was possible at the "Tempietto" of Cividale, where the documented use of vegetal aggregates in the plasters, including cotton filaments, made it possible to highlight the probable presence of Middle Eastern workers acting in the decoration, with their own techniques and with materials not in use in the West, like cotton [29].

The stucco decoration of Brescia has long been linked to that of the "Tempietto di Cividale", essentially contemporary. The presence of oriental workers at work in important Longobard royal construction sites [30] was invoked both from a stylistic point of view and from the composition of the stucco itself. In the case under analysis, the investigations on the stucco highlighted how it is practically pure gypsum, with responses very close to the stoichiometric value (0.7) of calcium sulphate. Even at the "Tempietto" of Cividale, the stuccos examined were all based on pure gypsum. This element would seem to provide a significant comparison in the stucco execution techniques of the two construction sites, which distance themselves from the Roman and late ancient tradition that included lime-based stucco or, at most, lime and gypsum. The exclusive use of gypsum, however, has always been more widespread in the Eastern Mediterranean, and certainly, was now prevalent in early medieval Western construction sites [30]. However, the lack of further discriminating technical elements, as observed for the pictorial technique used in Cividale [29] does not allow, at the current state of research, further deductions to better characterize the workers at work in the crypt of S. Salvatore in Brescia.

Acknowledgements This work has been performed under the concession of "Ministero della Cultura– Soprintendenza Archeologia, Belle Arti e Paesaggio per le Province di Bergamo e Brescia" (0014967 del 20/07/2022). Photos of the crypt fall under their concession and cannot be reproduced by any means. We are grateful to the AGLAE laboratory at the Louvre Museum in Paris, for their hospitality and technical and financial support. We are grateful to Dr. L. Negretti for her kind assistance during the SEM analyses.

Author contribution Alessandro Zucchiatti coordinated the research together with Stefano Roascio. Took part to the sampling on site and to all the analytical processes and discussions, being specifically responsible for the PIXE and SEM data processing. He also coordinated the edition of the article. Stefano Roascio coordinated the research together with Alessandro Zucchiatti. Took part to the sampling on site and was responsible of the historical and archaeological part of the work. He also participated to the discussion of the entire set of data, in particular from the archaeological and historic point of view. He also participated to the edition of the article. Inmaculada Donate Carretero was responsible of the Raman analyses and contributed to the discussion of the entire set of data and the article edition. Paolo Triolo organised and executed the photographic documentation of the crypt and the analyses with NIR and VIL techniques. He also contributed to the discussion of the entire set of data, in particular from the point of view of the art history and the article edition.

Funding Open access funding provided by University of the Witwatersrand. None of the authors has financial or non-financial interests that are directly or indirectly related to the work submitted for publication.

Data Availability statement The only additional data are PIXE concentration values that can be delivered in an excel file on request to the corresponding author. The rest of the data is included in the manuscripit. Figures concerning the crypt cannot be replicated without the permission of the of "Ministero della Cultura—Soprintendenza Archeologia, Belle Arti e Paesaggio per le Province di Bergamo e Brescia".

Open Access This article is licensed under a Creative Commons Attribution 4.0 International License, which permits use, sharing, adaptation, distribution and reproduction in any medium or format, as long as you give appropriate credit to the original author(s) and the source, provide a link to the Creative Commons licence, and indicate if changes were made. The images or other third party material in this article are included in the article's Creative Commons licence, unless indicated otherwise in a credit line to the material. If material is not included in the article's Creative Commons licence and your intended use is not permitted by statutory regulation or exceeds the permitted use, you will need to obtain permission directly from the copyright holder. To view a copy of this licence, visit http://creativecommons.org/licenses/by/4.0/.

References

1. UNESCO, 2012. "The Longobards in Italy, places of the power", in Unesco Heritage List Nomination Format, 2011.
2. M. De Paoli, "Strutture architettoniche e restauri", in Santa Giulia di Brescia: la cripta di San Salvatore. Hortus Artium Medievalium **23**, 140 (2017)
3. GP. Brogiolo, 2001. "Gli edifici monastici nelle fasi altomedievali", in San Salvatore - Santa Giulia a Brescia (a cura di Renata Stradiotti) , Skira, Milano, 2001.
4. A. Zucchiatti, S. Roascio, GP. Brogiolo, G. Gheroldi, M. Ibsen, 2007. "PIXE analysis of pictorial materials from the crypt of San Salvatore of Brescia (VIII century)", Minbar el Jaamia n.7, Actes de la RIPAM 2005, Meknes, Maroc.
5. T. Calligaro, J.C. Dran, E. Ioannidou, B. Moignard, L. Pichon, J. Salomon, Development of an external beam nuclear microprobe on the AGLAE facility at the Louvre museum. Nucl. Instr. Meth. **161–163**, 328–332 (2000)
6. J.L. Campbell, T.L. Hopman, J.A. Maxwell, Z. Nejedly, The Gueplh PIXE package II: alternative proton database. Nucl. Instr. and Meth. **B170**, 193–204 (2000). ((**and references therein**))
7. A. Bouquillon, J. Castaing, J. Salomon, F. Lucarelli, P.A. Mandò, P. Prati, A. Zucchiatti, 2001, "Iba Techniques to Study Renaissance Pottery Techniques", In: Connel, S.H., Tegen, R., (eds) *Proceedings of the International Conference on Fundamental & Applied Aspects of Modern Physiscs,* Luderitz 13–17 November 2000, World Scientific, Singapore, pp. 441–444
8. A. Zucchiatti, A. Bouquillon, J. Salomon, J.R. Gaborit, Study of Italian renaissance sculptures using an external beam nuclear microprobe. Nucl. Instr. Meth. **B161–163**, 699–703 (2000)
9. A. Zucchiatti, A. Bouquillon, G. Lanterna, F. Lucarelli, P.A. Mandò, P. Prati, J. Salomon, M.G. Vaccari, PIXE and μ-PIXE analysis of glazes from terracotta sculptures of the della Robbia workshop. Nucl. Instr. And Meth. **B189**, 358–363 (2002)
10. R.H Brill, "Chemical Analyses of Early Glasses, vol. 2 Table of Analyses", pg. 527–544, The Corning Museum of Glass, Corning, New York, 1999
11. Schott. https://www.us.schott.com/shop/advanced-optics/en/Matt-Filter-Plates/N-WG280/c/glass-N-WG280
12. G. Verri, "Visible-induced luminescence (VIL) imaging for the non-invasive characterisation of Egyptian blue: the case of an ancient Greek painted marble basin", accepted for publication within the framework of the NARNIA European Project 2014
13. J. Dyer, G. Verri; J. Cupitt "Multispectral Imaging in Reflectance and Photo-Induced Luminescence Modes: A User Manual"; Online: European CHARISMA Project; The British Museum: London, UK, 2013; pp. 122–151
14. J. Dyer, J. Cupitt, G. Verri, *Multispectral imaging in reflectance and photo-induced luminescence modes: a user manual* (The British Museum, London, 2013), pp.135–150
15. G. Verri, D. Saunders "Xenon flash for reflectance and luminescence (multispectral) imaging in cultural heritage applications", The British Museum Technical Bulletin, 8, 2014, 83–92.
16. G. Pozza, D. Ajò, G. Chiari, F. De Zuane, M. Favaro, Photoluminescence of the inorganic pigments Egyptian blue, han blue and han purple. J. Cult. Herit. **1**, 393–398 (2000)
17. P.L. Mora, P. Philippot, 1977. "La conservation des peintures murales", Bologna, ed. Compositori, pp. 48–59.
18. C. Coupry, 2001. "Les matériaux: support, enduits, pigments, liants", in S. Colinart, M. Menu, La matière picturale : fresque et peinture murale, Bari, Edipuglia, pp. 22–23.
19. A. Zucchiatti, P. Prati, A. Bouquillon, Characterisation of early medieval frescoes by μ-PIXE, SEM and Raman spectroscopy. Nucl. Instr. Meth. **B219–220**, 20–25 (2004)
20. A. Fanost, A. Gimat, L. de Viguerie, P. Martinetto, A.C. Giot, M. Clémancey, G. Blondin, F. Gaslain, H. Glanville, Ph. Walter, G. Mériguet, A.L. Rollet, M. Jaber, Revisiting the identification of commercial and historical green earth pigments. Colloids Surf. A **584**, 124035 (2020)
21. C. Grissom in "Artists' Pigments. A Handbook of their History and Characteristics" Robert L. Feller, Editor National Gallery of Art, Washington Archetype Publications, London 2012 pg. 160
22. D. Hradil, A. Píšková, J. Hradilová, P. Bezdička, G. Lehrberger, S. Gerzer, Mineralogy of bohemian green earth pigment and its microanalytical evidence in historical paintings. Archaeometry **53**, 563–586 (2011)
23. F. Ospitali, D. Bersani, G. Di Lonardo, P.P. Lottici, Green earths': vibrational and elemental characterization of glauconites, celadonites and historical pigments. J. Raman Spectrosc. **39**, 1066–1073 (2008)
24. A. Coccato, J. Jehlicka, L. Moensc, P. Vandenabeele, Raman spectroscopy for the investigation of carbon-based black pigments. J. Raman Spectrosc. **46**, 1003–1015 (2015)
25. M.C. Caggiani, A. Cosentino, A. Mangone, Pigments Checker version 3.0, a handy set for conservation scientists: a free online Raman spectra database. Microchem. J. **129**, 123–132 (2016)
26. E. Tomasini, E.B. Halac, M. Reinoso, E.J. Di Liscia, M.S. Maier, Micro-Raman spectroscopy of carbón-based pigments. J. Raman Specrosc. **43**, 1671–1675 (2012)
27. E. Tomasini, G. Siracusano, M.S. Maier, Spectroscopic, morphological and chemical characterization of historic pigments based on carbon. paths for the identification of an artistic pigment. Microchem. J. **102**, 28–37 (2012)
28. P. Triolo, "Manuale pratico di documentazione diagnostica per immagine per i BB.CC.", Il Prato, Saonara, 2019, pp.125–126.
29. A. Cagnana, A. Zucchiatti, S. Roascio, P. Prati, A. D'Alessandro, Indagini archeometriche sui materiali da costruzione del "Tempietto" di Santa Maria in Valle di Cividale del Friuli. I parte: gli affreschi altomedievali. Archeologia dell'Architettura, VIII **2003**, 69–87 (2003)
30. P. Casadio, T. Perusini, P. Spadea, Zur Stuckdekoration des "Tempietto Longobardo" in Cividale: technische und naturwissenschaftliche untersuchungsergebnisse, Stuck 1996, pp. 37–51.